Multi-scale reduced-order model of composite microstructure based on X-ray micro-CT imaging

Anna Madra, Kangning Su, Jing Du, Michael Hillman

CSMA 2019
14ème Colloque National en Calcul des Structures
13-17 Mai 2019, Presqu'île de Giens (Var)

Multi-scale reduced-order model of composite microstructure based on X-ray micro-CT imaging

A. Madra[1], K. Su[2], J. Du[2], M. Hillman[1]

[1] *CEE, The Pennsylvania State University, {amadra,mhillman}@psu.edu*
[2] *MNE, The Pennsylvania State University, {kxs535,jingdu}@psu.edu*

Résumé — In the process of Data-Driven modeling of the material microstructures, a reduced-order representation is preferred, as it is more manageable from the numerical standpoint. Its main drawback though is the loss of the connection between the parameters of the reduced-order model and the physical properties of the microstructure. We propose a methodology for exploring the intrinsic dimensionality of the multi-scale shape-manifold models of a heterogeneous material and point-out how the representativity of both geometric and spatial features changes depending on snapshot selection. The process is illustrated for an X-ray micro-CT scan of a polymer-ceramic composite microstructure.
Mots clés — Data-driven models, reduced-order modeling, composites.

1 Introduction

Volume imaging methods such as X-ray micro-CT enable the construction of realistic, numerical representations of the experimental material microstructure. While full-resolution reconstructions are the most accurate, their memory requirements are usually prohibitive for the purposes of numerical simulation and a reduced-order model is sought for instead. A successful approach to achieve low-dimensional representations of geometry by combining Singular Value Decomposition (SVD) with shape manifold interpolation has been proposed in [1, 2, 3]. The method is very effective in capturing the geometry of single-scale features, such as the surface of the impression left by the indenter [4] or a mesoscale envelope of a woven reinforcement in composites [5]. This efficiency is mainly because a low-rank reconstruction captures dominant features at a given scale and discards the higher-rank fluctuations. How this approach performs for microstructures possessing different spatial and geometric features at multiple scales remains unexplored. Here, by modifying the snapshot size we unravel the relations between low-rank features and physically semantic characteristics of the material, such as the shape and spatial distribution gradient of filler particles.

The rest of this paper is organized as follows : first the pre-processing of the X-ray micro-CT scans is briefly outlined and the acquisition of snapshots is described. Then, a reduced-order model is constructed through incremental Singular Value Decomposition and a low-rank manifold fitted with Diffuse Approximation (DA). Finally, the influence of snapshot size is investigated in relation to feature representativity and accuracy of the reconstruction. The conclusion sums up the current limitations of the method and proposes future expansion and applications.

2 Data pre-processing

2.1 Material and image acquisition

The material subject to investigation is an epoxy (Epo-tek 301) composite with a filler of alumina particles (Al_2O_3, Saint-Gobain, grit size 150). While the total filler fraction was 35% by weight, it is distributed with a gradient varying in the x direction (Fig. 1a). The specimen tested was a cuboid of dimensions $20 \times 5 \times 5$ mm^3. Further manufacturing parameters are detailed in [6, 7]. The X-ray micro-CT scans were performed on a GE v|tome|x L300 nano/microCT at the Penn State Center for Quantitative Imaging. The scan at a resolution of 6 μm, yielded 1214 tomogram slices, i.e., two-dimensional 32-bit grayscale images of 917×980 pixels in size.

2.2 Image processing

In transmission X-ray microcomputed tomography (X-ray micro-CT), the internal 3D microstructure of the material is revealed by imaging the distribution of the coefficient of attenuation μ defined in the Beer-Lambert's law [8]. At lower beam energies, as is the case here, the value of μ is directly related to the atomic number of a given phase in the material. A tomographic scan $\mathcal{T}$ is a 3D array representing $\mu(x,y,z)$ where $x = 1,\ldots,N_x$, $y = 1,\ldots,N_y$, $z = 1,\ldots,N_z$.

Here, we chose to explore the filler phase as it is the element of the microstructure displaying a high degree of variability, it will be considered for the data-driven model. To isolate it from other phases in the material (epoxy and air), a segmentation of the scan is necessary. The goal of the segmentation is to obtain a partition of all pairs of μ values and locations (x,y,z) into classes corresponding to particular phases ω

$$\mu(x,y,z) \mapsto \omega_{phase}. \tag{1}$$

Here, a supervised clustering Fast-Random-Forest (FRF) algorithm [9] has been applied yielding segmentation shown in Fig. 1b.

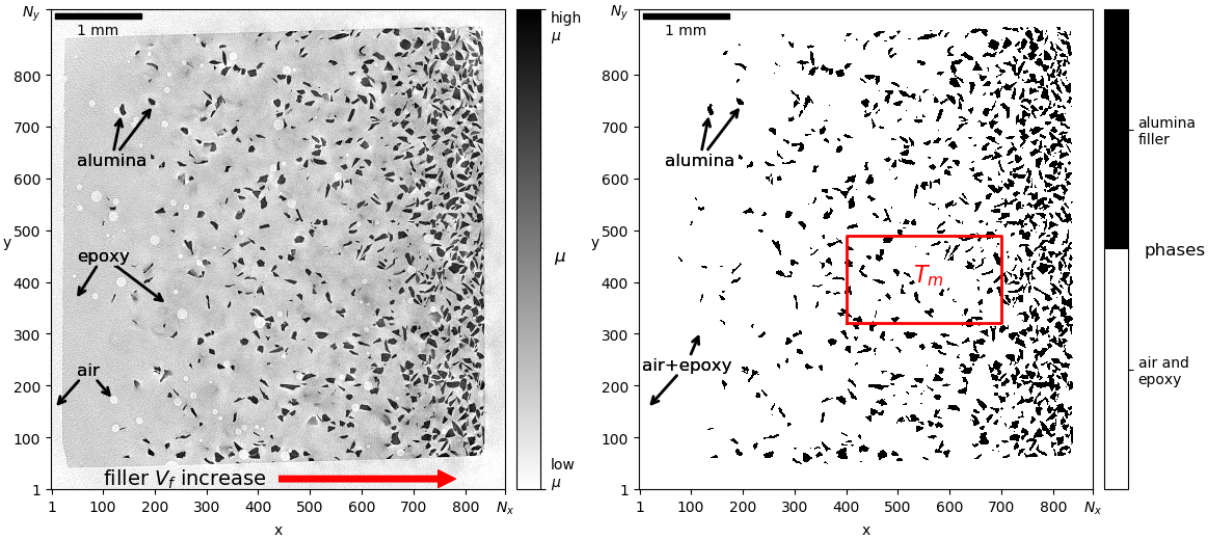

(a) Raw tomogram slice $\mathcal{T}_{xyz}$ for $z = 1$.

(b) Tomogram slice for $z = 1$ after segmentation.

FIGURE 1 – X-ray micro-CT data preprocessing for Data-Driven modeling.

2.3 Snapshot acquisition

To construct a reduced-order model of the material, we will take subsets T_m of different dimensions $n_x \times n_y \times n_z$ of the tomographic scan $\mathcal{T}$. For simplicity, only 2D slices of $\mathcal{T}$ will be considered, where in each subset $z = const$. Thus

$$\text{card}[T_m] = n_x \cdot n_y \cdot 1 = N \tag{2}$$

with N - the dimensionality of the subset, and M - number of subsets : $1 \leq M \leq N_x \cdot N_y$, reaching in size from the entire 2D slice to individual pixels.

Two types of features are extracted from each subset T_m. Firstly, a measure of filler volume fraction V_f is considered both for the entire T_m

$$V_f = \frac{\text{card}[\mu(x,y,z) \in \omega_{filler}]}{n_x \cdot n_y} \tag{3}$$

and also locally at the left and right extreme of the region T_m (Fig. 2a) as given by

$$V_{fl \text{ or } fr} = \frac{\text{card}[\mu(x,y,z) \in \omega_{filler}]}{n_x \cdot n_y \cdot \eta} \tag{4}$$

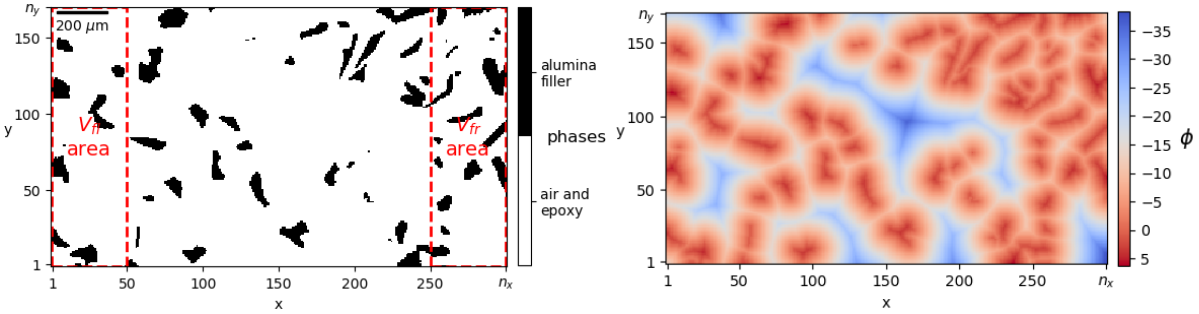

(a) Subset T_t with indicated areas for calculation of V_{fl} and V_{fr}.

(b) Level-set ϕ of T_m.

FIGURE 2 – Two types of microstructural features extracted from a tomogram subset T_m shown in Fig. 1b.

where $\eta \in <0,1>$ is a factor determined empirically and

$$\begin{aligned} x = 1,\ldots,n_x\cdot\eta,\ y = 1,\ldots,n_y,&\ \text{for the left extreme } V_{fl},\\ x = n_x - n_x\cdot\eta,\ldots,n_x,\ y = 1,\ldots,n_y,&\ \text{for the right extreme } V_{fr}. \end{aligned} \tag{5}$$

Secondly, we will consider snapshots s_m of the level-set function $\phi(x,y,z)$ of T_m defined as

$$\begin{cases} \phi > 0, & \text{if inside the particle,}\\ \phi = 0, & \text{if on the surface/outline of the particle,}\\ \phi < 0, & \text{if outside of the particle.} \end{cases} \tag{6}$$

Since tomographic scans $\mathcal{T}$ are represented as discrete 3D arrays, ϕ can be efficiently approximated using the fast marching method [10] (Fig. 2b).

3 Reduced-order model

3.1 Incremental SVD

All snapshots s_m

$$s_m = \begin{bmatrix} \vdots \\ \phi(x,y,z) \\ \vdots \end{bmatrix} \in \mathbb{R}^N \tag{7}$$

where $m = 1,\ldots,M$ are collected in a matrix of snapshots S

$$S = \begin{bmatrix} s_1 & \cdots & s_m & \cdots & s_M \end{bmatrix} \in \mathbb{R}^{N\times M}. \tag{8}$$

To represent all s_m in a common feature-space, we perform a Singular Value Decomposition (SVD) of the snapshot matrix

$$S = U\Sigma V^* \tag{9}$$

where Σ – diagonal matrix of singular values, and U, V – orthonormal basis of M snapshots, s.t.

$$U = \begin{bmatrix} u_1 & \cdots & u_M \end{bmatrix}. \tag{10}$$

Since tomographic data leads to large $N \times M$ values requiring high memory storage capacity, the SVD decomposition may be intractable. The key issue is the identification of only those snapshots that contribute significantly to the creation of the new basis. Thus, we will consider $R << M$ snapshots that are chosen following the incremental SVD algorithm in [11] yielding a reduced-order basis U_R. All snapshots s_m are then projected into the new, reduced-order shape-space (see Fig. 3 for $R = 3$)

$$A = \begin{bmatrix} \mathbb{\alpha}^{(1)} & \cdots & \mathbb{\alpha}^{(R)} \end{bmatrix}, \ \mathbb{\alpha}^{(r)} = \begin{bmatrix} \alpha_1^{(r)} \\ \vdots \\ \alpha_R^{(r)} \end{bmatrix}. \tag{11}$$

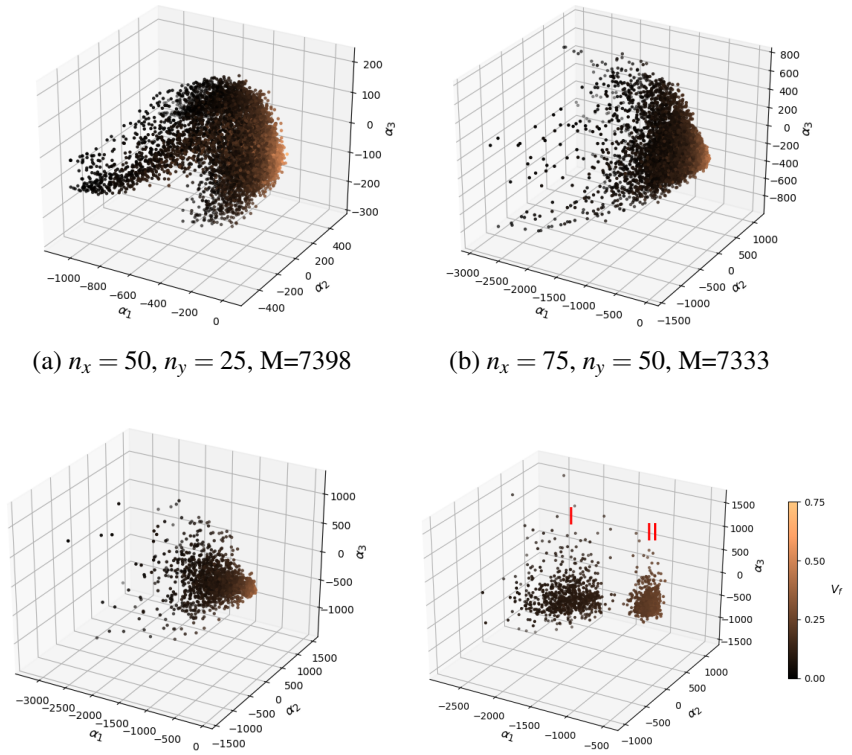

(a) $n_x = 50$, $n_y = 25$, M=7398 (b) $n_x = 75$, $n_y = 50$, M=7333

(c) $n_x = 100$, $n_y = 75$, M=1620 (d) $n_x = 200$, $n_y = 150$, M=1440

FIGURE 3 – Snapshots s_m of different subset T_m dimensions $n_x \times n_y$ projected into the reduced feature space $R = 3$. The colors correspond to the filler volume fraction V_f of the T_m. In (d) two distinct clusters *I* and *II* are indicated.

3.2 Shape manifold representation

To further reduce the amount of data required to represent the microstructure, we will search for a low-dimensional shape manifold

$$\mathcal{M}(\mathbb{\alpha}) = 0, \ \mathcal{M} \in \mathbb{R}^R \tag{12}$$

that represents all possible microstructures within the admissible range of values of $\mathbb{\alpha}$. It can be approximated as

$$\psi(\mathbb{\alpha}) = p^T(\mathbb{\alpha})a(\mathbb{\alpha}) \tag{13}$$

where p are polynomial basis functions and a are coefficients minimizing the weighted moving least squares criterion

$$J(a(\mathbb{\alpha})) = \frac{1}{2} \sum_{\mathbb{\alpha}^{(r)} \in V(\mathbb{\alpha})} w(\mathbb{\alpha}^{(r)}, \mathbb{\alpha})(p^T(\mathbb{\alpha}^{(r)})a - \mathbb{\alpha}^{(r)})^2 \tag{14}$$

with a neighborhood $V(\mathbb{\alpha})$ defined by the radius of influence $d^{(r)}$ of point $\mathbb{\alpha}^{(r)}$ and the weighting function w, e.g.

$$w(\mathbb{\alpha}^{(r)}, \mathbb{\alpha}) = \exp\left(-\frac{||\mathbb{\alpha}^{(r)} - \mathbb{\alpha}||}{2d^{(r)}}\right). \tag{15}$$

Here, this concept has been illustrated for three-dimensional manifolds that can be visualized (Fig. 4), although the intrinsic dimensionality will vary depending on the scale, as will be shown in the sequel.

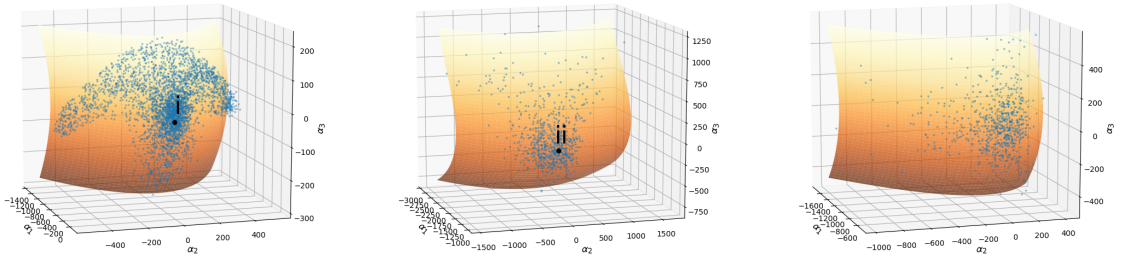

(a) $n_x = 50$, $n_y = 25$ (b) Cluster I, $n_x = 200$, $n_y = 150$ (c) Cluster II, $n_x = 200$, $n_y = 150$

FIGURE 4 – Manifold $\mathcal{M}(\mathbb{\alpha})$ fitted to projected snapshots s_m for different dimensions $n_x \times n_y$ of subset T_m.

4 Influence of snapshot size

4.1 Feature representativity

Two features are considered here as key in material model formulation : level-set on segmented subsets of the X-ray microtomographic scan, and global and local filler volume fraction measurements. In Fig. 3, four different sizes of subset T_m are explored in conjunction with the global V_f in T_m. Clearly, $\mathbb{\alpha}_1$ is directly tied to the V_f value, regardless of the subset size. On the other hand, the intrinsic dimensionality of projected samples increases significantly with larger subset sizes, beginning with a 2D surface for 50×25 (Fig. 3a), and subsequently turning into a seemingly random cloud (Fig. 3c) or multiple clouds (Fig. 3d) of points. This change in dimensionality can be attributed to the increasing importance of the variation in spatial organization of the specimen, better captured by the larger subsets. Thus, a smaller subset describes particle shape and volume fraction, while a larger one adds information on the spatial distribution. The main question is then : how to separate the large-scale effects of density gradient from the micro-scale parameters of the microstructure ?

In Fig. 3d it can be observed that a larger snapshot size not only increased the dimensionality of the model, but also separated the snapshots into two distinct classes. The observation of the V_f gradient made by comparison of the V_{fr} values in Fig. 5 indicates that V_{fr} is a major cause for the clustering. Although, this separation is also evident for V_f in Fig. 3d for the same subset dimensions, it does not manifest for V_{fl} (Fig. 5b), where the average V_{fl} for both clusters remains similar.

One way to diminish the influence of V_{fr} on the reduced-order model formulation, or to essentially separate it as a large-scale feature, is to classify the snapshots and find distinct shape manifolds for each of the clusters. This strategy has been employed here with V_{fr} used as a criterion for unsupervised classification with a k-means algorithm. Then new orthogonal bases U_R^I and U_R^{II} have been constructed for the clusters I and II, yielding a projection into a new feature space where a 2D surface fit was possible (Fig. 4b-4c), spanning all admissible values of V_{fr} used for the manifold interpolation.

It should be noted, that for smaller subsets, the gradient of V_f remains observable, with the highest values of V_{fl} and V_{fr} present at the opposite edges of the projected snapshots (Fig. 5a and 5c respectively). However, since the snapshots are smaller, the observed gradient is smoother than for larger subsets.

Hence even for smaller snapshots, all three features : V_f, V_{fl}, and V_{fr} together can be used to guide the construction of a shape manifold (Fig. 4a), but only if the density gradient remains relatively continuous.

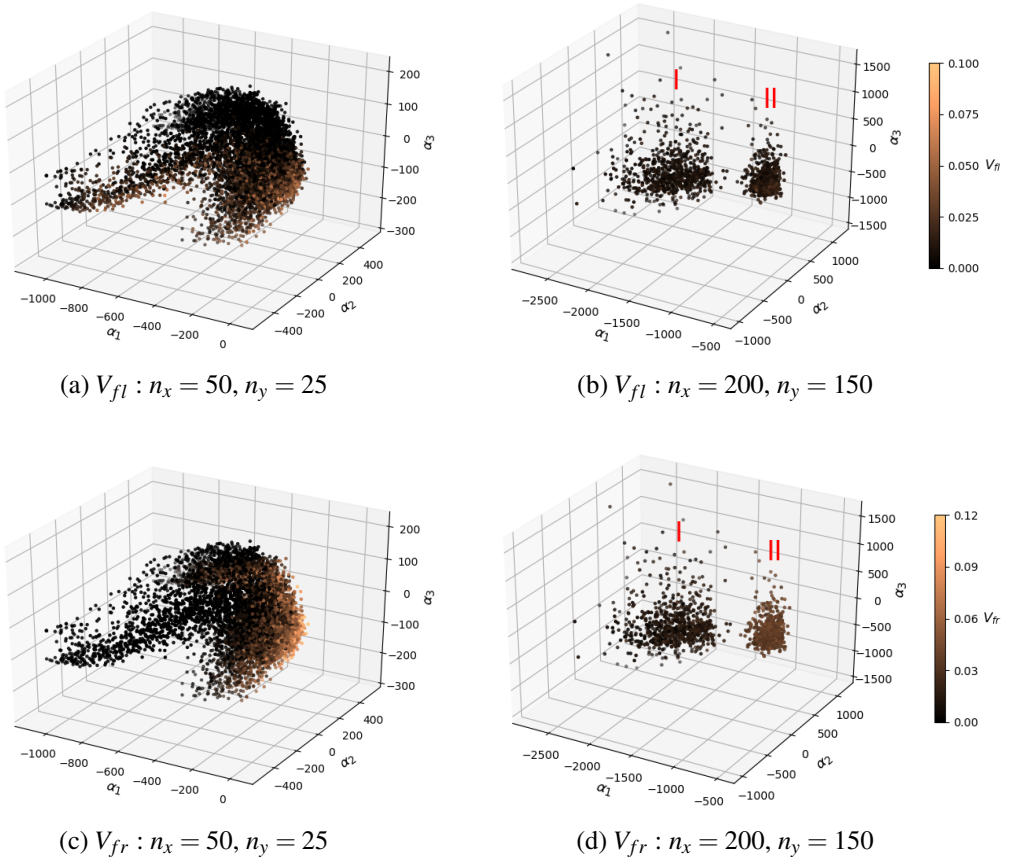

(a) V_{fl} : $n_x = 50$, $n_y = 25$

(b) V_{fl} : $n_x = 200$, $n_y = 150$

(c) V_{fr} : $n_x = 50$, $n_y = 25$

(d) V_{fr} : $n_x = 200$, $n_y = 150$

FIGURE 5 – Filler volume fraction (a-b) V_{fl} and (c-d) V_{fr} of projected snapshots s_m for two different dimensions $n_x \times n_y$ of subset T_m.

4.2 Accuracy of the reconstruction

The size of a snapshot apart from influencing the representativity of the features, also plays a major role in the overall performance of the proposed methodology. The original unsegmented scan requires > 4 GB of memory. After segmentation and by storing as compressed images (.png), this requirement goes down to ~ 23 MB. This is a number manageable for the purposes of morphological measurements and qualitative 3D analysis. For larger scans or scan time-series (*in-situ*), this number may increase drastically, thus the interest for a low-dimensional manifold representation.

A subset of size 50×25 yields snapshots of length $N = 1250$ required to describe the microstructure (Fig. 6a). A reconstruction plausibly indicating spatial filler distribution is achievable with a manifold of dimension $R = 15$ (Fig. 6b ; 1.2% of the entire set), and the reconstruction retaining both distribution and shape of the filler requires $R = 175$ (Fig. 6c ; 14%). A larger subset is originally described with snapshots with $N = 30\,000$ (Fig. 6d), but a plausible reconstruction is achievable with $R = 400$ (Fig. 6f ; 1.3%). This represents a significant reduction in memory requirements, especially if the same approach is considered for 3D subsets.

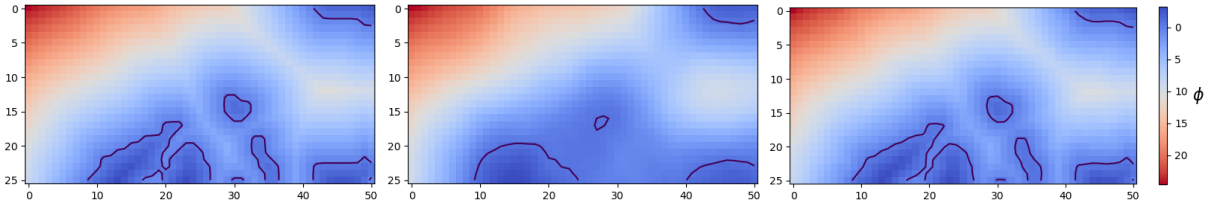

(a) Original snapshot at point i, $N = 1250$ (b) i reconstruction with $R = 15$. (c) i reconstruction with $R = 175$.

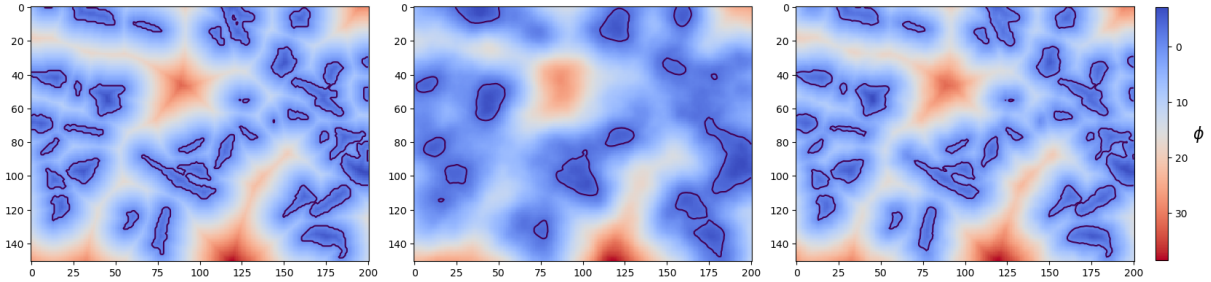

(d) Original snapshot at point ii, $N = 30\,000$. (e) ii reconstruction with $R = 100$. (f) ii reconstruction with $R = 400$.

FIGURE 6 – Original microstructure and reconstructions of snapshots at points i (Fig. 4a) and ii (Fig. 4b) for a varying dimensionality R of the shape manifold.

5 Conclusions

The impact of snapshot selection on the reduced-order data-driven model formulation has been explored. Despite being presented only for 2D subsets of the tomographic scan, the method can be easily adapted to 3D. The main challenge is to imbue the lower dimensional representations with a strong connection to physical parameters, such as attempted here : α_1 is clearly equivalent to V_f. At the same time, the connection of other features with those used for low-rank decomposition will require a careful investigation and classification of snapshots prior to the SVD to emphasize the representativity of physical features in the reduced-order space. The full exploration of the changes in dimensionality related to the snapshot size and selection are currently underway.

The further applications of the reduced-order model are multiple. First of all, an in-depth, structured conceptual model of the microstructure is created. This enables formulation of quantitatively sound observations of the impact of manufacturing and design parameters on material morphology. Secondly, a shape-manifold model is useful for generating new microstructures within the admissible range, especially those that were not subject to experimental examination. The validity of the manifold interpolation as opposed to other methods of interpolation is the subject of the ongoing work.

Acknowledgments

We would like to thank the U.S. National Science Foundation and Oak Ridge Associated Universities for the financial support of this work.

Références

[1] Balaji Raghavan, Piotr Breitkopf, Yves Tourbier, and Pierre Villon. Towards a space reduction approach for efficient structural shape optimization. *Structural and Multidisciplinary Optimization*, 48(5) :987–1000, 2013.

[2] Liang Meng, Piotr Breitkopf, Guenhael Le Quilliec, Balaji Raghavan, and Pierre Villon. Nonlinear Shape-Manifold Learning Approach : Concepts, Tools and Applications. *Archives of Computational Methods in Engineering*, pages 1–21, 2016.

[3] Anna Madra, Piotr Breitkopf, Alain Rassineux, and François Trochu. Image-based model reconstruction and meshing of woven reinforcements in composites. *International Journal for Numerical Methods in Engineering*, 112(9) :1235–1252, nov 2017.

[4] Liang Meng, Balaji Raghavan, Olivier Bartier, Xavier Hernot, Gerard Mauvoisin, and Piotr Breitkopf. An objective meta-modeling approach for indentation-based material characterization. *Mechanics of Materials*, 107 :31–44, 2017.

[5] Anna Madra, Piotr Breitkopf, Balaji Raghavan, and François Trochu. Diffuse manifold learning of the geometry of woven reinforcements in composites. *Comptes Rendus Mecanique*, 2018.

[6] J. Du, X. Niu, N. Rahbar, and W. Soboyejo. Bio-inspired dental multilayers : Effects of layer architecture on the contact-induced deformation. *Acta Biomaterialia*, 9(2) :5273–5279, 2013.

[7] Jing Du, Xinrui Niu, and Wole Soboyejo. Creep-assisted slow crack growth in bio-inspired dental multilayers. *Journal of the Mechanical Behavior of Biomedical Materials*, 46 :41–48, 2015.

[8] J. Baruchel, J.Y. Buffiere, E. Maire, Paul Merle, and Gilles Peix. X Ray Tomography in Material Science. page 204, 2000.

[9] L Breiman. Random forests. *Machine learning*, 45(1) :5–32, 2001.

[10] J.A. Sethian. A Fast Marching Level Set Method for Monotonically Advancing Fronts. *Proceedings of the National Academy of Sciences of the United States of America*, 93(4) :1591–1595, 1996.

[11] P Phalippou, S Bouabdallah, P Breitkopf, and P Villon. 'On the fly' snapshot selection for hyper-reduced Proper Orthogonal Decomposition with application to nonlinear dynamic. In *6th European Conference on Computational Mechanics*, number June, Glasgow, 2018.